

Low-Cost and Real-Time Industrial Human Action Recognitions Based on Large-Scale Foundation Models

Wensheng Liang^{a,1}, Ruiyan Zhuang^{b,1}, Xianwei Shi^b, Shuai Li^c, Zhicheng Wang^d and Xiaoguang Ma^{d,**}

^aSchool of Mechanical Engineering and Automation, Northeastern University, Wenhua Road, Heping District, Shenyang, 110819, Liaoning, China

^bIndustrial AI Technology Research Institute, Midea Intelligent Manufacturing Research Center, Shunde District, Foshan, 528311, Guangdong, China

^cFoshan Graduate School of Innovation, Northeastern University, Shunde District, Foshan, 528311, Guangdong, China

^dCollege of Information Science and Engineering, Northeastern University, Wenhua Road, Heping District, Shenyang, 110819, Liaoning, China

ARTICLE INFO

Keywords:

Industrial human action recognition
Large-scale foundation models
Low-cost

ABSTRACT

Industrial managements, including quality control, cost and safety optimization, etc., heavily rely on high quality industrial human action recognitions (IHARs) which were hard to be implemented in large-scale industrial scenes due to their high costs and poor real-time performance. In this paper, we proposed a large-scale foundation model(LFSM)-based IHAR method, wherein various LFSMs and lightweight methods were jointly used, for the first time, to fulfill low-cost dataset establishment and real-time IHARs. Comprehensive tests on in-situ large-scale industrial manufacturing lines elucidated that the proposed method realized great reduction on employment costs, superior real-time performance, and satisfactory accuracy and generalization capabilities, indicating its great potential as a backbone IHAR method, especially for large-scale industrial applications.

1. Introduction

With the rapid development of intelligent manufacturing, industrial human action recognitions (IHARs) drew great attentions [19] and started to play important roles in many industrial scenarios, such as quality control [21], safety monitoring [2], and process optimization [6]. Nevertheless, as IHAR scale increased in practice, the growing diversity of industrial actions involved in manufacture lines (MLs) raised complexity of data distribution and transferability across different MLs.

Constructing a generic industrial dataset for IHAR model training was challenging or even unrealistic [1], and up until now, annotating manually was still a mainstream approach for obtaining high quality industrial data, especially when supervised deep learning(DL) models were used. This made it very costly to employ conventional DL-Based IHAR methods, especially when dealing with large-scale industrial data. [5] proposed a framework of weakly supervised learning with attention architecture to partially alleviate high annotation costs (ACs). However, this method did not fully capture the diversity and complexity of corresponding features, and limited training data could easily lead to poor generalization across real-industrial scenarios. Conventional IHAR methods usually used small-scale detectors, e.g. YOLOv5 [8], and small-scale classifiers, e.g. ResNet-18 [10], to fulfill real-time IHAR [1]. In fact, these compact modules only exhibited high accuracy on limited industrial

scenarios, while retraining was usually required to avoid overfitting when scenarios changed. An effective approach to reduce the indirect ACs from retraining was to enhance model's generalization capabilities. However, minimizing the ACs of IHAR and maximizing their generalization ability was still an open and unsolved issue.

Recently emerging large-scale foundation models (LSFMs) were promising for the above-mentioned issues due to their powerful generalization capabilities. The LSFMs used multi-billion parameters for pre-training, allowing them to represent more complex relationships within inputs over conventional models. Moreover, the cross-modal capabilities of some LSFMs had potentials to simplify and automate the process of data labeling and dataset establishment, both of which were critical for IHAR employment.

In this paper, we proposed a LFSM-based low-cost and real-time industrial human action recognition (LRIHAR) model, with the least human intervention. Grounding DINO[14] and BLIP2[12] were used for action detection and recognition of large-scale industrial human actions, respectively. After obtaining sufficient boxed action pictures, YOLOv5 was trained as the detector for real deployment. In order to get high accuracy, we trained ViT-L for classification using low-rank adaptation (LoRA) fine-tuning method[11]. Finally, knowledge distillation (KD) [7] was used to distill a ViT-S model for low call time and high generalization to classify actions selected from YOLOv5. To summarize, our main contributions were:

- Grounding DINO and BLIP2 was jointly used to facilitate automatic annotations and industrial dataset establishment, wherein annotation costs was saved by more than 80% with superior generalization over traditional methods, speeding up IHAR dataset establishment process.

This work was supported in part by Initiation Funding of Foshan Graduate School of Innovation, Northeastern University (200076421002).

** Corresponding author.

✉ 2200385@stu.neu.edu.cn (W. Liang); zhuangry@midea.com (R. Zhuang); shixw4@midea.com (X. Shi); 2270882@stu.neu.edu.cn (S. Li); 2390108@stu.neu.edu.cn (Z. Wang); maxg@mail.neu.edu.cn (X. Ma)

ORCID(s): 0000-0001-8848-4166 (X. Ma)

¹These authors contributed equally to this work.

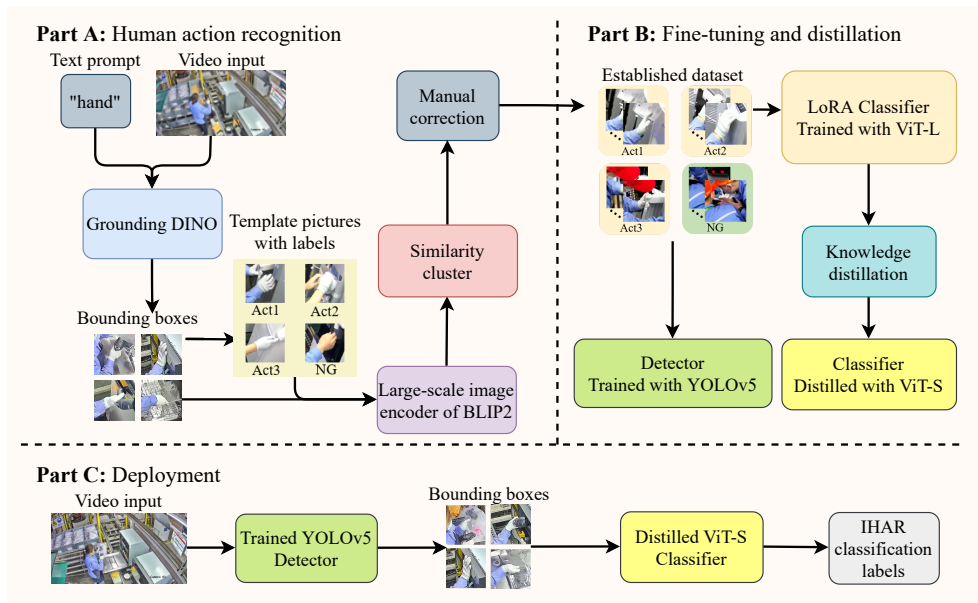


Figure 1: Workflow of the industrial human action recognition deployment process.

- LoRA and KD was used to reduce time for training and response, respectively, wherein 96.84% classification accuracy was achieved, outperforming pretrained ResNet-18 in all scenarios with call time less than 10ms, realizing real-time IHAR.
- Comprehensive experiments on large scale industrial data from three industrial MLs of Midea Group showed that the LRIHAR achieved 98.19% detection accuracy on average, and surpassed the conventional ResNet-18 by 4.4% on classification accuracy. Moreover, the LRIHAR showed superior AC cost saving, real-time performance, and generalization capabilities, simultaneously, facilitating its applications in large scale industrial scenarios.

2. Related work

2.1. Low-Cost Challenges of IHAR

For industrial MLs, the costs of IHAR were predominantly affected by dataset establishment and extensive training [20]. Different from a prevalent strategy utilizing large-scale video databases like UCF101 and Kinetics to construct non-industrial IHAR datasets [15], specific industrial data required to be collected to ensure better alignment with corresponding industrial requirements. In fact, the establishment of large-scale IHAR datasets required a substantial volume of video clips with expensive annotation interpretation and high quality variation across MLs, causing high employment costs.

In reality, IHAR annotation could be a time-consuming and costly task. According to our statistics, a human annotator would spend 4 hours on selecting 500 action bounding boxes as ground truth from the 100,000 frames collected to train the action detector model for this scenario. ACs also

occurred in transferring the same IHAR system to different MLs, i.e., scene switching. Although typical DL methods were suitable to achieve low-cost automatic annotations for non-industrial scenarios, such as [4], [3], there were limited investigations into automatic annotation in complex industrial scenarios, wherein ACs, detection, and classification accuracy needed to be jointly considered to achieve low-cost automatic annotating for industrial applications.

Emerging LSFMs had powerful generalization and zero-shot capability in various downstream tasks, such as sequence labeling [16] and question answering [18]. Various fusion of LSFMs had been proposed for target object detection, e.g. CLIP [17], ViLD [9], RegionCLIP [23], GLIP [13], and DINO [22]. In fact, the latest Grounding DINO [14] could reach 52.5 AP on COCO minival testing set and 63.0 AP after fine-tuning without any training set. Moreover, in response to the modality gap between fusion of LSFMs, [12] proposed BLIP2 wherein a bridge-connected form of Q-Former module was used to obtain remarkable performance on vision question answering tasks. By combining the above LSFMs, automatic label annotations and dataset establishment of IHAR could be realized.

2.2. Real-Time Implementation Challenges of IHAR

Real-time performance also posed a significant challenge in IHAR. In reality, high complexity and large parameter size of detection and classification models of IHAR usually brought inference delays, limiting its accessibility and scalability.

With increasing transferability requirements of industrial MLs, it could be promising to use the LSFMs as action classifiers to replace typical DL models like ResNet-18. However, re-training the LSFMs for new industrial scenes usually caused severe overfitting without sufficient scale of

industrial data, and re-training all parameters was infeasible for industrial deployment, also making it hard to achieve real-time performance.

LoRA[11], a parameter-efficient fine-tuning approach, used low-rank matrices decomposition to compress inter-layer weights, and the compressed matrices could better data for fine-tuning and keep the original feature extraction ability. This could help reduce the inference time cost on training the LSFMs. KD [7] was another approach to address real-time and lightweight challenges, wherein student models (smaller models) were created to mimick the behaviors of teacher models (the LSFMs) in order to compress the parameter size of the models.

3. Methodology

3.1. Automatic Annotation Process for IHAR Based on LSFMs

IHAR models that performed well on publically available datasets usually failed in industrial scenes, due to insufficient training on corresponding industrial datasets. Moreover, the high cost and low efficiency of manual annotations, which were common for building industrial datasets and conventional HAR models, i.e., YOLOv5, and ResNet-18, prevented them from meeting the real-time requirements of industrial production. To cope with this issue, we proposed to use the LSFMs for automatically building IHAR datasets.

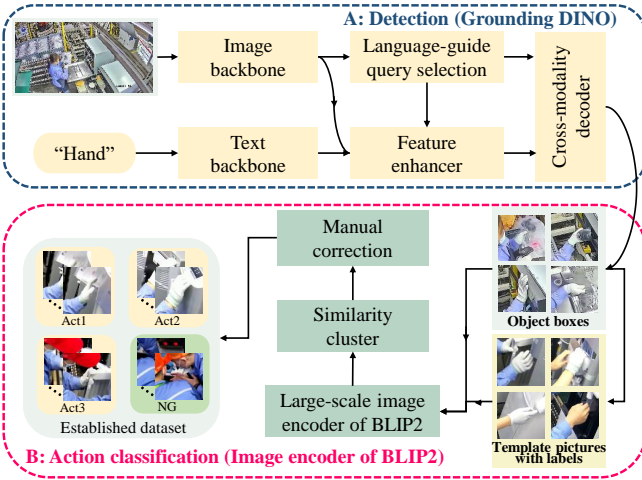


Figure 2: Dataset establishment processes of the industrial human action recognition.

3.1.1. Action Sifting and Detection

Grounding DINO was a zero-shot object detector proposed by Liu et al. [14], aiming to detect target objects in images through input text, wherein a dual-encoder-single-decoder architecture was adopted. As illustrated in Fig. 2A, image features and text features were initially extracted using an image backbone and a text backbone, respectively. The features were then input into a feature enhancer module to obtain cross-modality feature, wherein a language-guided module was utilized to select cross-modality queries.

Subsequently, these cross-modality queries were fed into a cross-modality decoder to detect desired features. The output queries from the decoder layer were used for predicting action bounding boxes.

3.1.2. Action Classification

Inspired by BLIP2 [12], we employed a frozen large-scale image encoder to perform action classification, as shown in Fig. 2B. Firstly, we selected several actions of each class as templates from Grounding DINO, and we constructed an NG class to store images that could not be fully matched with irrelevant actions, nonstandardized actions, and wrong images from Grounding DINO. Secondly, we input unlabeled actions and template action images into BLIP2 to get their corresponding semantic feature extraction, i.e., Q_1 and Q_2 , and their cosine similarity, i.e.,

$$\cos(\theta) = \frac{Q_1 \cdot Q_2}{\|Q_1\| \times \|Q_2\|}, \quad (1)$$

where \cdot represented the dot product of vectors, $\| \cdot \|$ represented their norms (lengths). Labels were assigned to the actions based on their similarity values.

In the similarity matching, we utilized a pre-defined threshold, denoted as λ , to help filter out objects with lower similarity and enhance the accuracy and reliability of the matching process. If the similarity exceeded λ , they were filtered out and considered as successful matches. Otherwise, they were classified as non-matches (NG class).

3.1.3. Manual correction

During actual deployment, a minimal amount of manual annotation was performed for the exclusion of erroneous data. Eventually, various actions and NG were classified for industrial dataset establishment.

3.2. Fine-tuning Process and Distillation

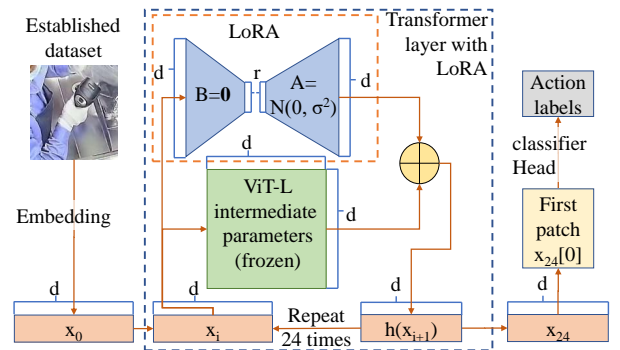


Figure 3: The LoRA fine-tuning process.

The fine-tuning process of LoRA was shown in Fig. 3 and,

$$h = W_0 x + B A x, \quad s.t. \begin{cases} B \in \mathbb{R}^{d \times r}, \\ A \in \mathbb{R}^{r \times k}, \\ r \ll \min(d, k), \end{cases} \quad (2)$$

where h represented the forward pass yields, W_0 represented the parameter matrix of each layer of the pre-trained ViT-L, and only A and B contained trainable parameters. Both W_0 and $\Delta W = BA$ were multiplied with the same input x and their respective output vectors were summed. After patch embedding and position embedding, the image embedded patches x_0 were fed into the first transformer block and LoRA module, simultaneously, wherein results were summed as h , i.e., x_1 , and then transferred to next layer, recursively. In order to maintain consistency in the input and output shapes of each layer for layer stacking, hyperparameters d and k were set to be equal. After 24 layers, the first patch of x_{24} was intercepted to classification head to predict action labels.

LoRA contained a dimension reduction matrix A and a dimension expansion matrix B , with the rank $r \ll \min(d, k)$, to maintain input and output dimensions, and avoid overfitting. The lower portion of the blue dashed frame in Fig. 3 displayed the pre-trained ViT-L, wherein d and k represented input and output dimensions, and weight dimensions, respectively. During training process, the parameters of the ViT-L model were frozen, and only matrices A and B were trained. The principle behind LoRA was to transform the high-dimensional parameter matrices of the model into lower-dimensional ones while preserving as much relevant information as possible. This reduced complexity and allowed faster fine-tuning of the LSFMs with a smaller number of parameters.

3.3. Actual Deployment

Although the LoRA fine-tuned ViT-L model could achieve relatively lower training time for LSFMs with satisfactory classification accuracy, it required a high response time comparing to traditional methods in practical deployment on MLs, and KD was used to solve this issue. For a smaller ViT-S model, which contained 16 transformer layers, we distilled it from ViT-L instead of training it from scratch. Specifically, the industrial dataset established in Section 3.1 underwent scaling transformations and data augmentation to align its data format with the trained ViT-L model. Then, using the same training loop, we distilled the student network ViT-S from the teacher network ViT-L. This approach allowed us to reduce model complexity and computing load with satisfactory performance.

The actual deployment diagram was illustrated in Part C of Fig. 1. In contrast to the action sifting and detection using Grounding DINO during automatic annotation process as shown in Part A, we employed the trained YOLOv5 on the constructed industrial dataset to reduce response time of detection. Subsequently, the distilled ViT-S model was adopted for response time reduction of action classification.

4. Experiments and Discussions

4.1. Experimental Setup

The LRIHAR was evaluated on three industrial datasets obtained from MLs in Midea Group, as listed in Table. 1,

Table 1
Datasets from three MLs

| GI-D | Action Name | Act1 | Act2 | Act3 | NG | |
|-------------------------|---------------------|------|------|------|-------|------|
| 3596 video frames | Template actions | 88 | 108 | 71 | 765 | |
| | Human actions | 682 | 833 | 125 | 15414 | |
| GI-WD | Action Name | Act1 | Act2 | Act3 | Act4 | NG |
| 3276 video frames | Template actions | 413 | 576 | 746 | 704 | 4089 |
| | Human actions | 1087 | 1168 | 1265 | 1272 | 1775 |
| GI-WH | Action Name | Act1 | Act2 | Act3 | NG | |
| 2295 video frames | Template actions | 150 | 9 | 73 | 464 | |
| | Human actions | 496 | 357 | 4863 | 10561 | |

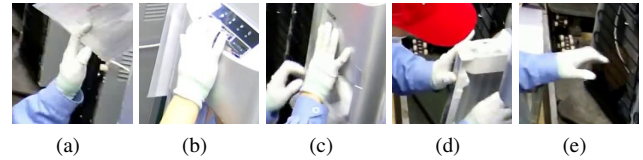


Figure 4: Typical human actions in general inspection posts in water dispenser ML (GI-WD). (a) Act1: instructions insertion, (b) Act2: top buttons pressing, (c) Act3: logo paste, (d) Act4: inner check, and (g) NG: other irrelevant actions.

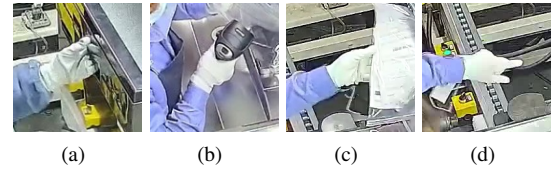


Figure 5: Typical human actions in general inspection posts in dishwasher ML (GI-D) (a) Act1: door O/C, (b) Act2: check, (c) Act3: instructions insertion, and (d) NG: other irrelevant actions.

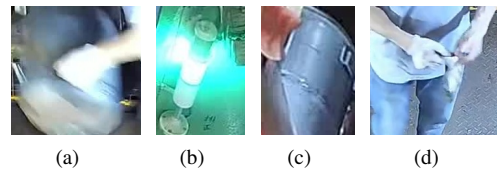


Figure 6: Typical human actions in test tank posts in water heater ML (TTP-WH). (a) Act1: heater tank lifting, (b) Act2: light, (c) Act3: heater tank localization, and (d) NG: other irrelevant actions.

i.e., general inspection posts in water dispenser ML (GI-WD), general inspection posts in dishwasher ML (GI-D), and test tank posts in water heater ML (TTP-WH), as shown in Figs. 4 to 6. We used a server with Intel(R) Xeon(R) Gold 6342 CPU @ 2.80GHz, 504GB of RAM, and NVIDIA A800 80G for distilling only, and the LRIHARs were trained,

Table 2

The results of accuracy and recall. Bold font was used to highlight the maximum recall value in each group.

| $T_{IoU} = 0.3$ | | | | |
|-----------------|----------------|---------------------------------|----------|---------------|
| Scenarios | Models | Hyperparameters | Accuracy | Recall |
| GI-WD ML | YOLOv5-G | Conf=0.1, NMS=0.9 | 90.10% | 75.94% |
| | YOLOv5-O | Conf=0.3, NMS=0.9 | 96.57% | 86.41% |
| | Grounding DINO | Box=0.3, Text=(from 0.1 to 0.9) | 72.67% | 89.36% |
| GI-D ML | YOLOv5-G | Conf=0.1, NMS=0.1 | 91.71% | 70.92% |
| | YOLOv5-O | Conf=0.1, NMS=0.9 | 89.05% | 81.74% |
| | Grounding DINO | Box=0.4, Text=(from 0.1 to 0.9) | 83.19% | 72.65% |
| TTP-WH ML | YOLOv5-G | Conf=0.1, NMS=0.1 | 51.74% | 22.13% |
| | YOLOv5-O | Conf=0.1, NMS=0.9 | 82.39% | 55.90% |
| | Grounding DINO | Box=0.4, Text=(from 0.1 to 0.9) | 89.94% | 81.83% |
| $T_{IoU} = 0.4$ | | | | |
| GI-WD ML | YOLOv5-G | Conf=0.3, NMS=0.2 | 92.92% | 71.18% |
| | YOLOv5-O | Conf=0.3, NMS=0.9 | 95.33% | 85.93% |
| | Grounding DINO | Box=0.3, Text=(from 0.1 to 0.9) | 67.61% | 87.32% |
| GI-D ML | YOLOv5-G | Conf=0.1, NMS=0.1 | 89.35% | 68.96% |
| | YOLOv5-O | Conf=0.3, NMS=0.9 | 93.60% | 75.49% |
| | Grounding DINO | Box=0.4, Text=(from 0.1 to 0.9) | 81.44% | 71.07% |
| TTP-WH ML | YOLOv5-G | Conf=0.1, NMS=0.9 | 50.45% | 23.00% |
| | YOLOv5-O | Conf=0.3, NMS=0.9 | 84.15% | 54.91% |
| | Grounding DINO | Box=0.4, Text=(from 0.1 to 0.9) | 89.69% | 81.40% |

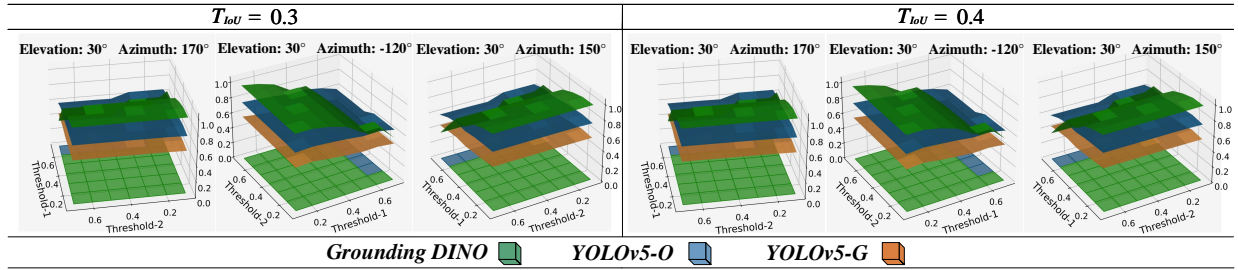


Figure 7: Recall surfaces under all hyperparameter combinations. In each plot, the vertical axis denoted accuracy or recall, while the two horizontal axes ranged from 0.0 to 1.0. We removed the fraction of values taken after 0.7, due to their extremely high accuracy and recall caused by too few predictions in all scenarios. To achieve a comprehensive surface analysis, we used three observation angles, i.e., elevation and azimuth, for each set of surface comparisons. At the same time, in order to better visualize the surface maximum value of the corresponding index on the three models, we projected the color of the model to the Threshold 1-Threshold 2 plane. Green, blue, and orange surfaces were generated by Grounding DINO, YOLOv5-O, and YOLOv5-G, respectively.

fine-tuned, and deployed with Intel Core i7-11700, 64GB of RAM, and NVIDIA GeForce RTX 2080 8G. We captured all videos using a DS-2CD3347DWDV3-L camera with a resolution of 2560*1440.

4.2. Action Detection across Multiple Industrial Scenarios

To verify generalization ability of the LSFMs for industrial dataset establishment, we used three trained models, i.e., Grounding DINO, YOLOv5-General (YOLOv5-G), and YOLOv5-Overfit (YOLOv5-O), to conduct comparative experiments, wherein both Grounding DINO and YOLOv5-G trained on publicly available datasets, and the YOLOv5-O trained on industrial data from the three MLs. Recall gauged the model's capacity to correctly detect all targets and was used as a crucial metric for measuring the model's

generalization ability in this paper, i.e.,

$$Recall = \frac{1}{N_t} \sum_j^{N_t} (\max(IoU_j) \geq T_{IoU}), \quad (3)$$

$$IoU_j = \{f_{IoU}(P_i, GT_j)\}_i^{N_p},$$

$$Accuracy = \frac{1}{N_p} \sum_i^{N_p} (\max(IoU_i) \geq T_{IoU}), \quad (4)$$

$$IoU_i = \{f_{IoU}(P_i, GT_j)\}_j^{N_t},$$

where N_p was the total numbers of the predicted bounding boxes given by specific model employed in the IHAR, N_t was the total numbers of ground true boxes, IoU_i was a set of values of intersection over union (IoU) calculated by the i_{th} predicted box and all ground true boxes, T_{IoU} was a pre-set IoU threshold for testing, f_{IoU} was a function used to

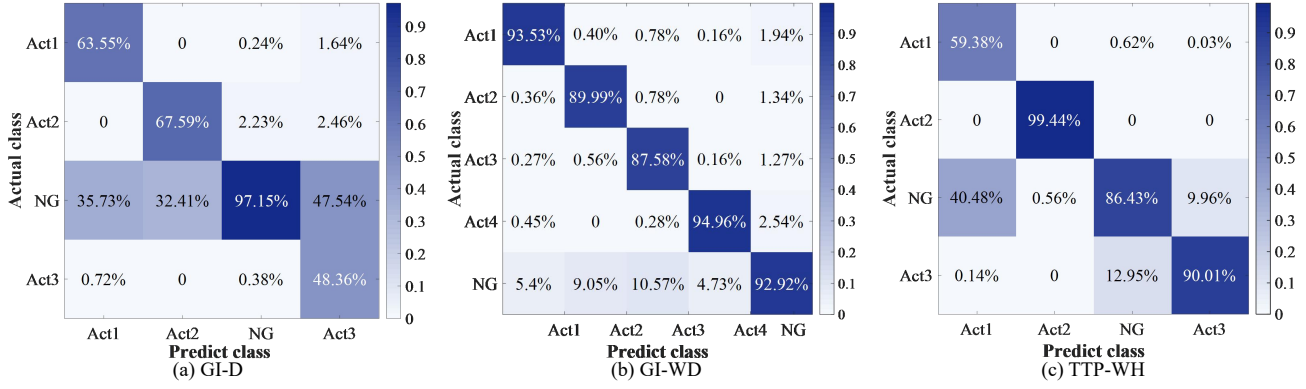


Figure 8: The confusion matrices of the LRIHAR for GI-D, GI-WD, and TTP-WH.

compute IoU , P_i was the i_{th} predicted box, and GT_j was the j_{th} ground true box, respectively.

Table 2 showed results of the accuracy and recall of the three models. It was noticed that two tunable hyperparameters were contained in the Grounding DINO, i.e., Box and Text and YOLO, i.e., Conf and NMS. The Grounding DINO was used to solve the low recall issues of YOLOv5-G in industrial scenes wherein specific actions were preferred to be detected as many as possible in order for IHAR systems to achieve high accuracy. In detection tasks, T_{IoU} was usually selected between 0.3 and 0.4. In fact, Table 2 showed that the recall of the Grounding DINO was 13.42% and 2.95% higher on the GI-WD ML and 59.70% and 25.93% higher on the TTP-WH ML, over the YOLOv5-G and YOLOv5-O when T_{IoU} was set to 0.3. Moreover, the recall of the Grounding DINO was 16.14% and 1.39% higher on the GI-WD ML and 58.40% and 26.49% higher on the TTP-WH ML, over the YOLOv5-G and YOLOv5-O, with T_{IoU} set to 0.4. Due to the fast handling actions in the GI-D ML, some images were blurred, and the positioning of the hand frames by the Grounding DINO had certain deviations, causing relatively poor recognition effect on the blurred scenarios. By adapting to various visual features and contexts, the Grounding DINO generalized its detection capabilities to unseen scenarios, facilitating its applications on object sifting and detecting, and enhancing the robustness and reliability of the IHAR system.

As shown in Table 2, the recall and accuracy performance of the YOLOv5-G was significantly lower than that of the YOLOv5-O, except for GI-D ML with T_{IoU} set to 0.3. Specifically, although the YOLOv5-O had been fed through industrial scenarios, the recall on TTP-WH ML was only 55.90% and 54.91% with T_{IoU} set to be 0.3 and 0.4, respectively, due to over-fitting, making manual intervention necessary to carry out data annotation for scenario changes when using YOLOv5-G. In fact, the YOLOv5-G only obtained 22.13% and 23.00% recall with T_{IoU} set to be 0.3 and 0.4, respectively, as shown in Table 2. This meant that it missed massive operational hand actions which were required for proper IHAR and these undetected objects had to be manually recalled.

Moreover, we also plotted all hyperparameter combinations to enable a more visual assessment of the three models. As shown in Fig. 7, by testing on three MLs, different recall surfaces were generated. Specifically, the YOLOv5-G demonstrated noticeably lower accuracy over the YOLOv5-O, while the Grounding DINO exhibited comparable or higher accuracy when only some hyperparameter combinations were selected. Moreover, Grounding DINO clearly demonstrated superior recall performance over the other two methods, indicating its strong generalization capabilities across different scenarios as a detection model. With suitable hyperparameters, the Grounding DINO could be directly applied to object sifting and detection of annotation systems, effectively reducing manual ACs and minimizing the risk of missing objects.

4.3. Action Classification through Image Encoder of BLIP2

Although the Grounding DINO could maintain a relatively high recall rate in various industrial scenes, there still existed a small numbers of detection errors. Therefore, we utilized a frozen large-scale image encoder from BLIP2 to classify the detected human actions, and to reduce the cost of industrial dataset establishment.

As shown in Fig. 8, confusion matrices on the three industrial datasets revealed that the target images detected by Grounding DINO and processed by BLIP2 could be accurately classified into the correct action types. It should be noted that the accuracy of various actions on the GI-D dataset was not particularly high. This was due to the fact that uncertain actions were categorized into the NG class and removed from the constructed industrial dataset.

The total action numbers in GI-D, GI-WD, and TTP-WH were 12148, with 11110 actions correctly classified, 39 actions incorrectly classified, and 1592 actions classified as the NG class, meaning that the LRIHAR achieved a 99.6% prediction accuracy in average on action classification without considering the NG class. The introduction of the NG class allowed effective exclusion of partially determined actions, thereby reducing subsequent manual correction cost.

Table 3

Comparisons of annotation costs (ACs) and detection accuracy under two annotation methods, wherein ACs contained the number of images to be manually annotated (annotation workload ,AW), and the time that was manually annotated (annotation time ,AT). ImpV represented the improvement of LRIHAR over manual annotation.

| ACs from a single ML | | | |
|------------------------|---|-------------------|-------------------------|
| Sources of costs | Indices of costs | Manual annotation | LRIHAR (ImpV) |
| ACs for entire IHAR | AW (images for all 20 posts in a single ML) | 2,000,000 | 1,000,000 (-50%) |
| ACs for detection | AW for training detector (images per post) | 500 | 100 (-80%) |
| | AT of entire detection tasks (hours per post) | 4 | 0.8 (-80%) |
| | AT of entire detection tasks (hours for all 20 posts in a single ML) | 80 | 16 (-80%) |
| ACs for classification | AW for training classifier (per action category for a post) | 200 | 20 (-90%) |
| | AT of entire classification tasks (hours per post) | 24 | 4 (-83.3%) |
| | AT of entire classification tasks (hours for all 20 posts in a single ML) | 480 | 80 (-83.3%) |
| Detection Accuracy | | 96.98% | 98.19% (+1.21%) |

4.4. ViT-L Fine-tuning and Distilling

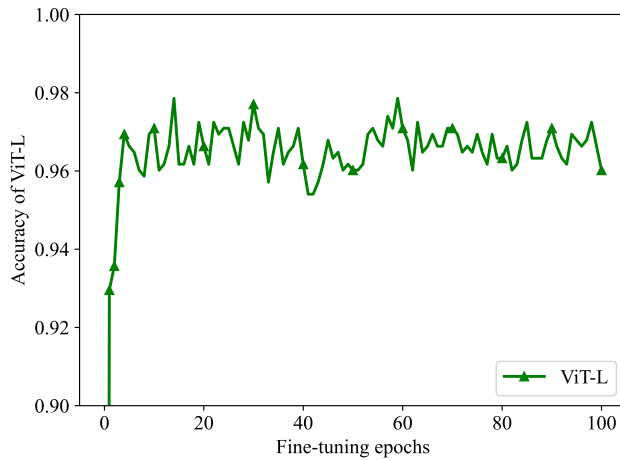


Figure 9: Fine-tuning accuracy rate curve of ViT-L. The average time for each fine-tuning epoch is 48 seconds.

To evaluate fine-tuning performance of ViT-L, we conducted long-time experiments and analyzed accuracy in different epochs, wherein parameters r , learning rate, and batch size were set to be 16, $5e-3$, and 64, respectively. In KD, we trained ViT-S for 100 epochs. The learning rate, batch size and teacher's temperature were set to $5e-3$, 1024, and 0.07, respectively.

The accuracy of fine-tuning ViT-L was plotted in Fig. 9, wherein the fine-tuning process experienced rapid accuracy increase in the first couple of epochs and maintained an average accuracy of 96.44% for the subsequent 90 epochs. Meanwhile, we selected the ViT-L with the highest accuracy from the first five epochs as a teacher to distill ViT-S. After distillation, the ViT-S achieved an accuracy of 96.84%, slightly higher than the average values of the fine-tuned ViT-L.

It is noticed that the ViT-L and its classifier head were jointly fine-tuned, and the first epoch did not yield satisfactory results as it mainly focused on training the classifier head. Hence, the ViT-L achieved high accuracy except for

the first few epochs, demonstrating that the low-rank characteristic of weight matrices of KD greatly reduced trainable parameters numbers and avoided overfitting efficiently.

4.5. Low-Cost and Real-Time Performance of the LRIHAR

Table. 3 showed annotation costs (ACs) for conventional method and LRIHAR, including the deployment expenditures for the entire IHAR, detection, and classification, wherein the conventional method manually annotated data as in most industrial annotation tasks.

In fact, we used 2,000,000 raw images from inspection posts (IPs) on a single ML per hour for comparison. The use of Grounding DINO in the LRIHAR could successfully filter out 1,000,000 images with high recall rate and accuracy since no actions were contained in these images. This reduced overall AW and automatically categorized the images without hand information into the NG class.

LRIHAR utilized Grounding DINO to automatically select 500 training images, with only 100 images requiring correction for detection. Meanwhile, only 0.8 hours were consumed for one IP and 16 hours for 20 IPs, i.e., 80% improvement over YOLOv5-G. As shown in Table. 3, ResNet-18 required 200 normal images for each target action category, similar to the training for detection. In reality, only 20 images were required to be manually corrected in these 200 normal images, and it successfully decreased time-consuming to 4 hours, one sixth of manual annotation. Considering 20 IPs as the benchmark for expansion, the process only required 80 hours, 83.3% shorter than 480 hours of manual annotation. It was also interesting to see that the accuracy of YOLOv5-O trained with datasets from LRIHAR was improved by 1.21%. These improvements under AC reduction attributed to the fact that both Grounding DINO and BLIP-2 applied in the LRIHAR had powerful generalization, making it possible to replace and outperform human workers in handling the alignment task between annotation and image semantics in industrial environments.

Table. 4 showed real-time performance for deploying various classifiers for the IHAR, including general ResNet-18, retrained ResNet-18, ViT-L, ViT-L + LoRA, ViT-S, and

Table 4

Comparisons of accuracy and time-consumption with various classifiers. Bold font represented the highest accuracy in the same ML scenario.

| Accuracy comparisons of various classifiers for single ML | | | | | | |
|---|-------------------|---------------------|--------|---------------|--------|---------------|
| | General ResNet-18 | Retrained ResNet-18 | ViT-L | ViT-L + LoRA | ViT-S | LRIHAR |
| GI-D ML | 92.94% | 93.13% | 94.41% | 95.92% | 95.26% | 97.80% |
| GI-WD ML | 91.10% | 94.15% | 94.82% | 95.75% | 95.46% | 95.98% |
| TTP-WH ML | 79.50% | 90.08% | 92.94% | 97.65% | 92.59% | 96.74% |
| Average | 87.85% | 92.45% | 94.06% | 96.44% | 94.44% | 96.84% |
| Time-consuming comparisons of training various classifiers for single ML (Real-time of real ML required to be less than 10ms) | | | | | | |
| | General ResNet-18 | Retrained ResNet-18 | ViT-L | ViT-L + LoRA | ViT-S | LRIHAR |
| Pre-training time (hours) | 0 | 12 | 0 | 0 | 0 | 48 |
| Fine-tuning time (s) | 30 | 30 | 30 | 240 | 30 | 240 |
| Algorithm call time (ms) | ≤10 | ≤10 | ≥200 | ≥200 | ≤10 | ≤10 |
| All training time for 20 posts (hours) | 0 | 240 | 0 | 0 | 0 | 48 |

LRIHAR. The time-consumption comparisons contained pre-training time for the backbone classifiers, fine-tuning time for the head of classifiers, and algorithm call time used to predict action labels. The general ResNet-18, ViT-L, and ViT-S did not require pre-training time due to the availability of public weight resources, and this consumption did not exist in ViT-L + LoRA due to the fact that the LoRA was a fine-tuning strategy. ResNet-18 and LRIHAR retrained the entire backbone of classifiers, and all classifiers in Table. 4 fine-tuned their head structures to adapt industrial data.

As shown in Table. 4, the LRIHAR achieved the highest average accuracy (96.84%) among all methods, wherein the accuracy reached 97.80% and 95.98% for GI-D and GI-WD ML, respectively, both higher than those of other methods in the same group. Although ViT-L + LoRA achieved 97.65% accuracy on TTP-WH ML, higher than that of the LRIHAR, it was not suitable for real employment since its call time was larger than 200ms, much longer than acceptable limitation of MLs, i.e., 10ms. Compared with general ResNet-18, retrained ResNet-18, and ViT-S that met the industrial real-time requirements, the LRIHAR surpassed them by 8.99%, 4.39%, and 2.44% on accuracy, respectively. Meanwhile, although the pre-training time of the LRIHAR was higher than retrained ResNet-18, the time-consuming did not increase with the expansion of IPs. As shown in Table. 4, for 20 IPs on a single ML, the LRIHAR only required 48 hours, while the retrained ResNet-18 required 240 hours. These results elucidated that LRIHAR provided superior accuracy over previous SOTA methods and maintained satisfactory call time to meet real industrial applications indicating its great potential as a general IHAR methods.

5. Conclusion

In this paper, we proposed a low-cost and real-time industrial human action recognition (LRIHAR), wherein Grounding DINO was used to replace YOLOv5 for automatic annotation in various industrial scenarios, BLIP2 was used to extract action feature and match with templates, and LoRA and KD was used to improve classification accuracy and compress model size. The proposed LRIHAR

allowed us to control labeling cost, call time consumption, and accuracy, simultaneously, indicating its great potential as a backbone, for large-scale industrial applications. In future work, we will focused on handling fine-grained and continuous HAR for industrial applications.

CRedit authorship contribution statement

Wensheng Liang: Experiments conduction, Software, Manuscripts drafting. **Ruiyan Zhuang:** Conceptualization of this study, Methodology, Coordination. **Xianwei Shi:** Data collection, Methodology, Software, Experimental verification. **Shuai Li:** Statistical analysis, Manuscripts drafting. **Zhicheng Wang:** Statistical analysis, Manuscripts drafting. **Xiaoguang Ma:** Structure conception of the manuscript, Revision of the manuscript.

References

- [1] Ahmad, H.M., Rahimi, A., 2022. Deep learning methods for object detection in smart manufacturing: A survey. *Journal of Manufacturing Systems* 64, 181–196.
- [2] Aiello, G., Catania, P., Vallone, M., Venticinque, M., 2022. Worker safety in agriculture 4.0: A new approach for mapping operator's vibration risk through machine learning activity recognition. *Computers and Electronics in Agriculture* 193, 106637.
- [3] Alshehri, A., Taïleb, M., Alotaibi, R., 2022. Deepaia: An automatic image annotation model based on generative adversarial networks and transfer learning. *IEEE Access* 10, 38437–38445.
- [4] Cao, J., Zhao, A., Zhang, Z., 2020. Automatic image annotation method based on a convolutional neural network with threshold optimization. *Plos one* 15, e0238956.
- [5] Chen, H., Hu, Q., Zhai, B., Chen, H., Liu, K., 2020a. A robust weakly supervised learning of deep conv-nets for surface defect inspection. *Neural Computing and Applications* 32, 11229–11244.
- [6] Chen, W., Liu, H., Qi, E., 2020b. Discrete event-driven model predictive control for real-time work-in-process optimization in serial production systems. *Journal of Manufacturing Systems* 55, 132–142.
- [7] Duval, Q., Misra, I., Ballas, N., 2023. A simple recipe for competitive low-compute self supervised vision models. *arXiv:2301.09451*.
- [8] G. Jocher, A. Chaurasia, A.S.e.a., 2022. ultralytics/yolov5: v7.0 - YOLOv5 SOTA Realtime Instance Segmentation. URL: <https://doi.org/10.5281/zenodo.7347926>, doi:10.5281/zenodo.7347926.

- [9] Gu, X., Lin, T.Y., Kuo, W., Cui, Y., 2021. Open-vocabulary object detection via vision and language knowledge distillation. arXiv preprint arXiv:2104.13921 .
- [10] He, K., Zhang, X., Ren, S., Sun, J., 2016. Deep residual learning for image recognition, in: Proceedings of the IEEE Conference on Computer Vision and Pattern Recognition (CVPR).
- [11] Hu, E.J., Shen, Y., Wallis, P., Allen-Zhu, Z., Li, Y., Wang, S., Wang, L., Chen, W., 2021. Lora: Low-rank adaptation of large language models. arXiv:2106.09685.
- [12] Li, J., Li, D., Savarese, S., Hoi, S., 2023. Blip-2: Bootstrapping language-image pre-training with frozen image encoders and large language models. arXiv preprint arXiv:2301.12597 .
- [13] Li, L.H., Zhang, P., Zhang, H., Yang, J., Li, C., Zhong, Y., Wang, L., Yuan, L., Zhang, L., Hwang, J.N., et al., 2022. Grounded language-image pre-training, in: Proceedings of the IEEE/CVF Conference on Computer Vision and Pattern Recognition, pp. 10965–10975.
- [14] Liu, S., Zeng, Z., Ren, T., Li, F., Zhang, H., Yang, J., Li, C., Yang, J., Su, H., Zhu, J., Zhang, L., 2023. Grounding dino: Marrying dino with grounded pre-training for open-set object detection. arXiv:2303.05499.
- [15] Liu, X., Pinteá, S.L., Nejadasl, F.K., Booi, O., Van Gemert, J.C., 2021. No frame left behind: Full video action recognition, in: Proceedings of the IEEE/CVF Conference on Computer Vision and Pattern Recognition, pp. 14892–14901.
- [16] Liu, Y., Meng, F., Zhang, J., Xu, J., Chen, Y., Zhou, J., 2019. Gcdt: A global context enhanced deep transition architecture for sequence labeling. arXiv preprint arXiv:1906.02437 .
- [17] Radford, A., Kim, J.W., Hallacy, C., Ramesh, A., Goh, G., Agarwal, S., Sastry, G., Askell, A., Mishkin, P., Clark, J., et al., 2021. Learning transferable visual models from natural language supervision, in: International conference on machine learning, PMLR. pp. 8748–8763.
- [18] Shao, Z., Yu, Z., Wang, M., Yu, J., 2023. Prompting large language models with answer heuristics for knowledge-based visual question answering, in: Proceedings of the IEEE/CVF Conference on Computer Vision and Pattern Recognition, pp. 14974–14983.
- [19] Sun, Z., Ke, Q., Rahmani, H., Bennamoun, M., Wang, G., Liu, J., 2022. Human action recognition from various data modalities: A review. IEEE Transactions on Pattern Analysis and Machine Intelligence , 1–20URL: <https://doi.org/10.1109/TPAMI.2022.3183112>, doi:10.1109/tpami.2022.3183112.
- [20] Vieira, J.C., Sartori, A., Stefenon, S.F., Perez, F.L., De Jesus, G.S., Leithardt, V.R.Q., 2022. Low-cost cnn for automatic violence recognition on embedded system. IEEE Access 10, 25190–25202.
- [21] Yan, J., Wang, Z., 2022. Yolo v3+ vgg16-based automatic operations monitoring and analysis in a manufacturing workshop under industry 4.0. Journal of Manufacturing Systems 63, 134–142.
- [22] Zhang, H., Li, F., Liu, S., Zhang, L., Su, H., Zhu, J., Ni, L.M., Shum, H.Y., 2022. Dino: Detr with improved denoising anchor boxes for end-to-end object detection. arXiv preprint arXiv:2203.03605 .
- [23] Zhong, Y., Yang, J., Zhang, P., Li, C., Codella, N., Li, L.H., Zhou, L., Dai, X., Yuan, L., Li, Y., et al., 2022. Regionclip: Region-based language-image pretraining, in: Proceedings of the IEEE/CVF Conference on Computer Vision and Pattern Recognition, pp. 16793–16803.